Dynamic measurement of cytosolic pH and [NO_3^-] uncovers the role of the vacuolar transporter AtCLCa in cytosolic pH homeostasis

Elsa Demes[a], Laetitia Besse[a], Paloma Cubero-Font[b], Béatrice Satiat-Jeunemaitre[a], Sébastien Thomine[a], and Alexis De Angeli[a,b,1]

[a]Institute for Integrative Biology of the Cell, Commissariat à l'Energie Atomique et aux Énergies Alternatives, CNRS, University Paris-Sud, Université Paris-Saclay, 91198 Gif-sur-Yvette Cedex, France; and [b]Biochemistry and Plant Molecular Physiolgy, University Montpellier, CNRS, Institut National de Recherche pour l'Agriculture, l'Alimentation et l'Environnement (INRAE), Montpellier SupAgro, 34060 Montpellier Cedex 2, France

Edited by Julian I. Schroeder, Cell and Developmental Biology Section, Division of Biological Sciences, University of California San Diego, La Jolla, CA, and approved May 19, 2020 (received for review April 24, 2020)

Ion transporters are key players of cellular processes. The mechanistic properties of ion transporters have been well elucidated by biophysical methods. Meanwhile, the understanding of their exact functions in cellular homeostasis is limited by the difficulty of monitoring their activity in vivo. The development of biosensors to track subtle changes in intracellular parameters provides invaluable tools to tackle this challenging issue. AtCLCa (*Arabidopsis thaliana* Chloride Channel a) is a vacuolar NO_3^-/H^+ exchanger regulating stomata aperture in *A. thaliana*. Here, we used a genetically encoded biosensor, ClopHensor, reporting the dynamics of cytosolic anion concentration and pH to monitor the activity of AtCLCa in vivo in *Arabidopsis* guard cells. We first found that ClopHensor is not only a Cl^- but also, an NO_3^- sensor. We were then able to quantify the variations of NO_3^- and pH in the cytosol. Our data showed that AtCLCa activity modifies cytosolic pH and NO_3^-. In an AtCLCa loss of function mutant, the cytosolic acidification triggered by extracellular NO_3^- and the recovery of pH upon treatment with fusicoccin (a fungal toxin that activates the plasma membrane proton pump) are impaired, demonstrating that the transport activity of this vacuolar exchanger has a profound impact on cytosolic homeostasis. This opens a perspective on the function of intracellular transporters of the Chloride Channel (CLC) family in eukaryotes: not only controlling the intraorganelle lumen but also, actively modifying cytosolic conditions.

nitrate | stomata | CLC | *Arabidopsis* | biosensor

The fluxes of ions between cell compartments are driven by membrane proteins forming ion channels, exchangers, symporters, and pumps. Defects in the transport systems residing in intracellular membranes result in major physiological failures at the cellular and the whole-organism levels (1). The localization of transport systems in intracellular membranes prevents the use of in vivo electrophysiological approaches, considerably limiting our understanding of their cellular functions. Among the different families of ion transporters identified, the CLC (Chloride Channel) family, which has been widely investigated in the last decades, constitutes a group of membrane proteins present in all organisms (2). The members of the CLC family function as anion channels or anion/H^+ exchangers sharing a similar structural fold (3, 4). In eukaryotes, all of the CLCs localized in intracellular membranes behave as anion/H^+ exchangers. In mammals, mutations in intracellular CLCs lead to severe genetic diseases affecting bones, kidneys, and the brain (2). In plants, CLCs regulate nutrient storage and photosynthesis and participate in drought and salt stress tolerance (5–11). In the last few decades, many studies addressed the biophysical properties of intracellular CLCs and provided a solid ground to understand the transport mechanisms of these exchangers (12–16). However, we still lack a molecular interpretation of the role of the CLC exchangers within cells, preventing a full understanding of the defects observed in organisms carrying mutations in *CLC* genes (2).

Plant guard cells (GCs) constitute an appropriate experimental model to unravel CLC functions at the subcellular level. In plants, GCs are specialized cells gating the stomata pores at the leaf surface. Their biological function relies on the regulation of ion transport systems residing in the plasma membrane (PM) and vacuolar membrane (VM) (17–19). The VM delimits the largest intracellular compartment of GCs, the vacuole (17, 20). Stomata control gas exchanges between the photosynthetic tissues and the atmosphere, including water loss by transpiration. Two GCs delimit the stomata pore and regulate its aperture according to environmental conditions. The regulation of the stomata pore aperture is based on the capacity of GCs to change their turgor pressure and consequently, their shape. Increase and decrease of the turgor pressure in GCs open and close the stomata, respectively. Turgor changes in GCs depend on the accumulation/release of ions into/from the vacuole. Therefore, vacuolar ion transporters are key actors of stomata responses. The identification of a growing number of ion transporters and channels that function in the VM of GCs highlighted the importance of intracellular transport systems selective for anions, such as NO_3^-, Cl^-, and malate^{2-}, and for cations, such as potassium (7, 8, 21–25).

Significance

Intracellular transporters are key actors in cell biological processes. Their disruption causes major physiological defects. Intracellular ion transporters are usually thought to control luminal conditions in organelles; meanwhile, their potential action on cytosolic ion homeostasis is still a black box. The case of a plant Chloride Channel (CLC) is used as a model to uncover the missing link between the regulation of conditions inside the vacuole and inside the cytosol. The development of an original live imaging workflow to simultaneously measure pH and anion dynamics in the cytosol reveals the importance of an *Arabidopsis thaliana* CLC, AtCLCa, in cytosolic pH homeostasis. Our data highlight an unsuspected function of endomembrane transporters in the regulation of cytosolic pH.

Author contributions: S.T. and A.D.A. designed research; E.D., L.B., P.C.-F., and A.D.A. performed research; E.D., L.B., P.C.-F., and A.D.A. analyzed data; and B.S.-J., S.T., and A.D.A. wrote the paper.

The authors declare no competing interest.

This article is a PNAS Direct Submission.

[1]To whom correspondence may be addressed. Email: alexis.deangeli@supagro.fr.

This article contains supporting information online at https://www.pnas.org/lookup/suppl/doi:10.1073/pnas.2007580117/-/DCSupplemental.

First published June 16, 2020.

Anion channel and transporter families such as Slow Activating Anion Channels (SLAC/SLAH), Aluminum Activated Malate Transporter (ALMT), and CLC strongly influence GC function and stomata responses to environmental changes (7, 21–23, 26–29). However, the observed GC phenotypes and the biophysical characteristics of these ion transport systems can be somehow difficult to reconcile (7, 8, 20, 21, 27, 30). The vacuolar CLC AtCLCa (*Arabidopsis thaliana* Chloride Channel a) is illustrative of this difficulty. AtCLCa is known to act as a $2NO_3^-/1H^+$ exchanger driving the accumulation of NO_3^- into the vacuole (6, 31), suggesting a role in stomata opening. However, analysis of GC responses from *AtCLCa* knockout plants revealed that AtCLCa is not only involved in light-induced stomata opening but also, in abscisic acid (ABA)-induced stomata closure (7). This intriguing dual role questions the molecular interpretation of the subcellular role of AtCLCa.

Being anion/H^+ exchangers, intracellular CLCs are expected to induce simultaneous modifications of $[NO_3^-]$, $[Cl^-]$, and pH in both the lumen of intracellular compartments and the cytosol. However, so far, only their role in regulating luminal-side conditions has been investigated in plants using isolated vacuoles (32) and in mammals in lysosomes and endosomes (14, 16, 33). In mammals, CLC-5 was shown to contribute to the acidification of endosomes (33), while CLC-7 activity was associated only with modest changes in lysosomal pH that could not be detected in all studies (16, 33). In both cases, the link between luminal acidification and the severe phenotypes observed in the corresponding knockout mice was not established (16, 33). In plants, no role of a CLC transporter in vacuolar pH regulation was so far demonstrated in vivo. Here, we hypothesized that AtCLCa activity affects cytosolic parameters in addition to its well-documented role in anion accumulation inside vacuoles. We therefore aimed to visualize whether the activity of an intracellular CLC like AtCLCa induces changes in the cytosolic pH and $[NO_3^-, Cl^-]$ dynamics in living GCs.

In order to be able to detect simultaneously the subtle changes in cytosolic pH and anion concentration induced by the activity of an intracellular transporter, we introduced the genetically encoded biosensor ClopHensor into GCs as an experimental model. ClopHensor is a ratiometric biosensor originally developed in mammalian cells with spectroscopic properties allowing us to measure $[Cl^-]$ and pH in parallel (34). Our results demonstrated that ClopHensor allows simultaneous measurements of the cytosolic pH, $[Cl^-]$ (34), and additionally, $[NO_3^-]$, which is an abundant anion in plant cells. We expressed ClopHensor in the cytosolic compartment (*cyt*) of *Arabidopsis* and conducted imaging experiments on GCs to visualize the subcellular effects of the activity of the NO_3^-/H^+ exchanger AtCLCa in vivo. We monitored by confocal laser scanning microscope (CLSM) the changes in $[Cl^-]_{cyt}$ or $[NO_3^-]_{cyt}$ in parallel with pH_{cyt}. We developed a specific image analysis workflow to measure the fluorescence ratios of interest in GCs. A comparative study between GCs from wild-type and AtCLCa knockout mutant plants shows that the vacuolar exchanger AtCLCa not only controls the kinetics of $[NO_3^-]_{cyt}$ changes but also, actively participates in the control of pH_{cyt}. These results highlight an unexpected role of AtCLCa in the regulation of pH_{cyt}. Furthermore, they open a perspective on the cellular functions of intracellular transporters in GCs that might provide an integrated framework to understand the function of intracellular CLCs in other eukaryotic cells.

Results

In Vitro Assays Reveal a Strong Affinity of ClopHensor for NO_3^-. In contrast to mammalian cells, several anionic species are present in the millimolar range in plant cells (5, 35). Therefore, we investigated the sensitivity of ClopHensor to Cl^-, NO_3^-, PO_4^{3-}, malate^{2-}, and citrate^{3-}, the main anions present in the model plant *Arabidopsis* (5). ClopHensor was previously shown to be insensitive to SO_4^{2-}, which also accumulates to millimolar levels in plant cells (34, 36). We used recombinant ClopHensor proteins bound to Sepharose beads and recorded the fluorescence upon exposure to a range of anions by CLSM after excitation at 458 nm (emission 500 to 550 nm), 488 nm (emission 500 to 550 nm), and 561 nm (emission 600 to 625 nm) (Fig. 1*A*). The ratio R_{anion} (F_{458}/F_{561}) was calculated from the ratio of the fluorescence intensity images after excitation at 458 nm (F_{458}) and 561 nm (F_{561}) to estimate the effect of anions on ClopHensor (*SI Appendix* has an R_{anion} calculation). No significant difference in R_{anion} was observed between the control ($R_{anion}^{ctrl} = 1.14 \pm 0.11$) and 30 mM PO_4^{3-} ($R_{anion}^{norm} = 0.88 \pm 0.05$), malate^{2-} ($R_{anion}^{norm} = 0.91 \pm 0.02$), and citrate^{3-} ($R_{anion}^{norm} = 0.92 \pm 0.05$) (Fig. 1*A*). Meanwhile, we found that ClopHensor was sensitive to Cl^- ($R_{anion}^{norm} = 0.42 \pm 0.03$) as previously reported (34) and remarkably, also to NO_3^- ($R_{anion}^{norm} = 0.21 \pm 0.03$) (Fig. 1*A*). ClopHensor displayed a higher affinity to NO_3^- ($K_d^{NO3} = 5.3 \pm 0.8$ mM at pH 7) than to Cl^- ($K_d^{Cl} = 17.5 \pm 0.5$ mM at pH 6.8) (Fig. 1*B*). The sensitivity range of ClopHensor was between 2 and 162 mM for Cl^- (at pH 6.8) and between 0.6 and 48 mM for NO_3^- (at pH 7) (Fig. 1*B*). Notably, in the physiological range of cytosolic pH (i.e., 6.8 to 8), the K_d^{NO3} of ClopHensor was between 5 and 25 mM (*SI Appendix*, Fig. S1), which is in the range of the previously reported $[NO_3^-]_{cyt}$ values of about 5 mM (35), therefore making it suitable to monitor the dynamics of this anion. Concerning chloride, K_d^{Cl} of ClopHensor was between 17.5 and 163 mM (*SI Appendix*, Fig. S1), values that are above the reported basal $[Cl^-]_{cyt}$ in plant cells of about 10 mM (37). To test the pH sensitivity of ClopHensor in our in vitro assays, we calculated the ratio R_{pH} (F_{488}/F_{458}) (*SI Appendix* has an R_{pH} calculation). In agreement with a previous report (34), we found a strong response of R_{pH} to pH variations with a steep dynamic range of ninefold change between pH 6.1 and pH 7.9 and a $pK_a = 6.98 \pm 0.09$ (Fig. 1*D*). Neither the binding of NO_3^- nor that of Cl^- modified significantly the pH sensitivity of ClopHensor (*SI Appendix*, Fig. S1), confirming its robustness as a dual anion and pH biosensor.

ClopHensor Is a Robust and Sensitive Sensor of Cytosolic pH in *A. thaliana* GCs. We generated transgenic *Arabidopsis* plants (ecotype Columbia 0 [Col-0]) expressing ClopHensor in the cytosol and nucleoplasmic compartments under the control of the Ubiquitin10 promoter (*pUB10*:*ClopHensor*). The expression of ClopHensor did not affect the development of the plants, indicating that its expression did not significantly interfere with the amount of anions available in the cytosol for cellular metabolism (*SI Appendix*, Fig. S2). To measure the pH sensitivity of ClopHensor in living GCs, stomata from *pUBI10*:*ClopHensor* were sequentially exposed to NH_4-acetate–based buffers to clamp the pH_{cyt} at defined values between 5 and 9 (Fig. 1 *C* and *D*). We found that ClopHensor sensitivities to pH in vivo and in vitro were very similar. The mean $<RpH_{cyt}>$, calculated from each pixel in the stomata, showed that the pH titration curve of ClopHensor in GCs mirrored the in vitro assay (Fig. 1*D*). The pK_a (6.98 ± 0.11) and the sensitivity range of ClopHensor (between pH 6.1 and 7.9) measured in vivo matched the values measured in vitro (Fig. 1*D*). These findings demonstrate that 1) ClopHensor is a reliable reporter for intracellular pH changes in GCs, 2) the cytosolic environment does not affect ClopHensor properties with respect to pH, and 3) the ClopHensor sensitivity range is appropriate for measuring pH_{cyt} in GCs.

Settings and Design of the Experimental Workflow in GCs. The data we obtained open the possibility of measuring the variations of $[NO_3^-]_{cyt}$, $[Cl^-]_{cyt}$, and pH_{cyt} in vivo. This provides a unique opportunity to disclose in living cells how ion fluxes across the PM and the VM of GCs affect cytosolic conditions. In order to

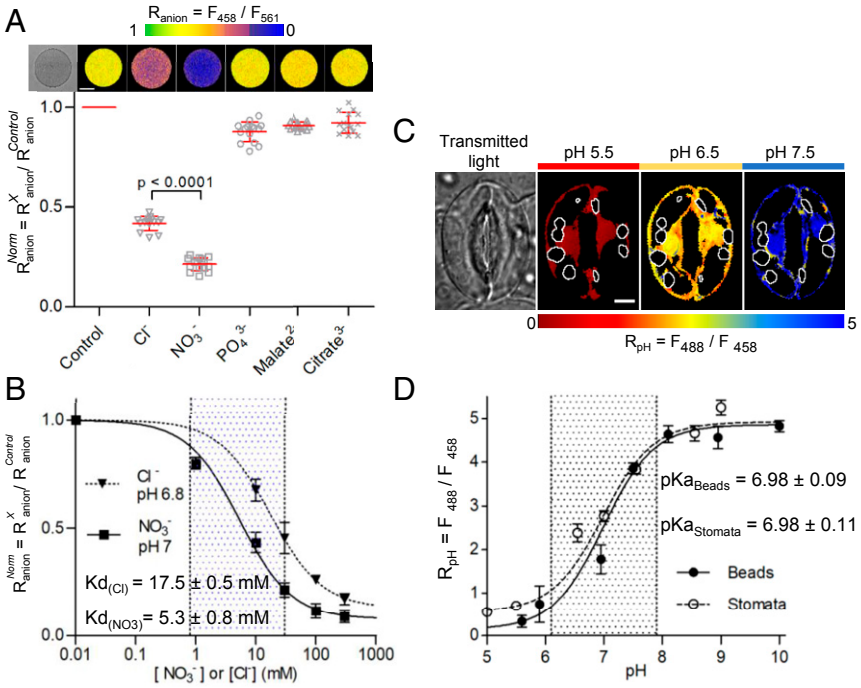

Fig. 1. ClopHensor is sensitive to NO_3^-, Cl^-, and pH. (*A* and *B*) In vitro ratio imaging of Sepharose beads decorated with ClopHensor in the presence of 30 mM Cl^-, NO_3^-, PO_4^{3-}, malate^{2-}, and citrate^{3-}. (*A*, *Upper*) False color images of representative beads displaying the fluorescence ratio R_{anion} ($R_{anion} = F_{458}/F_{561}$). (Scale bar: 50 μm.) (*A*, *Lower*) normalized $R^{norm}{}_{anion}$ (mean value ± SD; $n \geq 15$ beads in each condition). The bracket indicates a statistically significant difference. (*B*) In vitro dose–response analysis of ClopHensor showing $R^{norm}{}_{anion}$ in the presence of Cl^- or NO_3^- from 0 to 300 mM at pH 6.8 and 7, respectively (mean value ± SD; $n = 15$ beads in each condition). Data were normalized to control conditions and fitted with *SI Appendix*, Eq. **S2**. Dotted area, sensitivity range for NO_3^- (0.6 to 48 mM) of ClopHensor. (*C*) In vivo ratio imaging of *Arabidopsis* stomata expressing ClopHensor. False color images of a representative stomata showing the fluorescence ratio R_{pH} ($R_{pH} = F_{488}/F_{458}$) upon sequential exposure to NH_4-acetate buffers at pH 5.5, 6.5, and 7.5. From left to right, transmitted light and false color images of R_{pH} at pH 5.5, 6.5, and 7.5, respectively. White contours, localization of the chloroplasts subtracted during the analysis. (Scale bar: 5 μm.) (*D*) Plot of R_{pH} vs. pH showing that the pH dependence of ClopHensor in vivo (stomata; black circles; $n \geq 10$) and in vitro (Sepharose beads; white circles; $n \geq 15$) is comparable (mean value ± SD). Data were fitted with *SI Appendix*, Eq. **S1**. Dotted area, sensitivity range for pH (6.1 to 7.9) of ClopHensor.

quantify $[NO_3^-]_{cyt}$, $[Cl^-]_{cyt}$, and pH_{cyt} in GCs, we optimized the fluorescence acquisition protocol in GCs expressing ClopHensor (*SI Appendix*, Figs. S3 and S4) and determined the temporal window to set up our experiments. First, to maximize the collected fluorescence and minimize photodamage by the laser, we selected stable transgenic lines expressing *pUBI10*:*ClopHensor* with high fluorescence in GCs after excitation at 458 nm (emission 500 to 550 nm), 488 nm (emission 500 to 550 nm), and 561 nm (emission 600 to 625 nm). Second, to quantify $[NO_3^-]_{cyt}$, $[Cl^-]_{cyt}$, and pH_{cyt}, we excluded the fluorescent signals emitted by chloroplasts (excitation 488 nm, emission 650 to 675 nm). Therefore, we developed an image processing workflow to accurately measure ClopHensor fluorescence in the cytosol of plant cells (*SI Appendix*, Fig. S4).

To derive the $[NO_3^-]_{cyt}$, $[Cl^-]_{cyt}$, and pH_{cyt} in GCs, we used the calculation procedure described in Arosio et al. (34) (*SI Appendix*). To obtain a quantitative estimation of the changes in $[NO_3^-]_{cyt}$ and $[Cl^-]_{cyt}$ induced by the applied treatments, we determined in vivo the R_{anion} ratio in the absence of NO_3^- and Cl^- (i.e., R^0). R^0 is required to calculate the actual concentration of Cl^- and NO_3^- in the cytosol (*SI Appendix*). To this aim, we set up experimental conditions where the initial endogenous $[NO_3^-]_{cyt}$ and $[Cl^-]_{cyt}$ should be below the sensitivity threshold of ClopHensor. Selective microelectrode measurements have shown that, when plants are grown with less than 0.01 mM NO_3^- supply, the cytosolic levels are below 0.5 mM (38). Therefore, we grew *pUB10*::*ClopHensor* plants in vitro in an NO_3^--free medium (0 mM NO_3^- medium) and determined the whole-plant $[NO_3^-]$ and $[Cl^-]$ at different days after germination (DAG) (*SI Appendix*, Table S1). We found that, in these conditions, the whole-seedling endogenous content of NO_3^- and Cl^- was decreasing after germination. At DAG 14, Cl^- was no longer detectable; meanwhile, $[NO_3^-]$ was below the sensitivity threshold of ClopHensor (i.e., 0.6 mM at pH 7). Subsequently, based on these data, we imaged the fluorescence in stomata from *pUB10*:*ClopHensor* plants grown in vitro for 14 d on an NO_3^--free medium and measured a mean ratio $R^0{}_{anion}$ of 0.56 ± 0.07 ($n = 29$ stomata) (*SI Appendix*, Fig. S3*E*).

Dynamic Measurements of Cytosolic NO_3^-, Cl^-, and pH in *Arabidopsis* GCs. We challenged 14-d-old NO_3^--starved *Arabidopsis* seedlings expressing ClopHensor for the simultaneous detection in GCs of $[NO_3^-]_{cyt}$, $[Cl^-]_{cyt}$, and pH_{cyt} changes upon extracellular NO_3^- or Cl^- supply/removal (Fig. 2). The experimental design was based on the application of different extracellular conditions in a sequence of five steps (Fig. 2). GCs were 1) perfused with NO_3^--free medium to determine the ratio R^0 for each stomata; 2) exposed to 30 mM KNO_3 to observe $[NO_3^-]_{cyt}$ changes; 3) washed out with NO_3^--free medium; 4) exposed to 30 mM KCl to observe $[Cl^-]_{cyt}$ changes; and 5) washed out again with NO_3^--free medium. We applied 30 mM KNO_3 or KCl as these concentrations are commonly used in stomata aperture assays (8, 39). To perform a full experiment, we imaged GCs for 190 min, and each stomata was imaged every 4 min with sequential excitation at 561, 488, and 458 nm. Fluorescence intensity recorded in NO_3^--free medium was not altered after 190 min of illumination, indicating that ClopHensor was not significantly affected by photobleaching over the whole duration of the experiment (*SI Appendix*, Figs. S5 and S6). Raw data suggested striking variations of the mean fluorescence intensity recorded after excitation

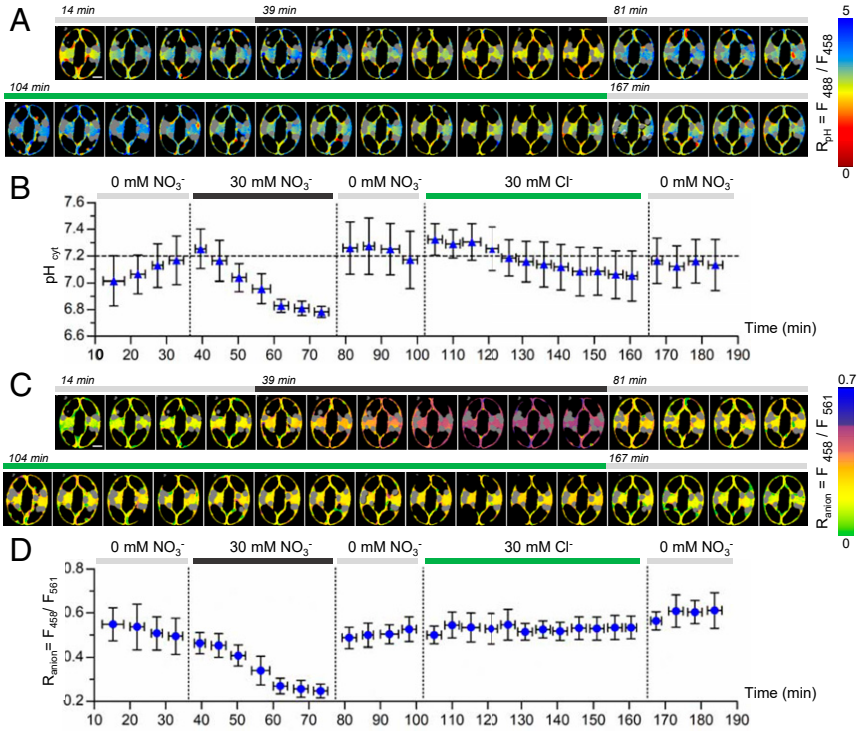

Fig. 2. ClopHensor reveals the dynamics of cytosolic pH, NO_3^-, and Cl^- in *Arabidopsis* stomata. Epidermal peels from plants grown in vitro for 14 d in NO_3^--free media were imaged (*SI Appendix*). (*A* and *C*) Representative false color ratio images of R_{pH} (*A*) and R_{anion} (*C*) at different time points of a stomata sequentially exposed to NO_3^--free medium (0 mM NO_3^-), 30 mM KNO_3, and 30 mM KCl. Gray areas, localization of chloroplasts subtracted during the analysis. (Scale bars: 5 μm.) (*B*) pH_{cyt} was quantified at each time point from the corresponding R_{pH} images. (*D*) Quantification of the R_{anion} in the cytosol of GCs. (*B* and *D*) pH_{cyt} (*B*) and R_{anion} (*D*), indicating $[NO_3^-]_{cyt}$, change simultaneously upon extracellular application and removal of 30 mM KNO_3. Horizontal error bars represent the time interval of 4 min for the sequential imaging of stomata. Data represent mean values ± SD ($n = 6$). *SI Appendix*, Fig. S4 shows the workflow for the calculation of pH_{cyt} (*B*) and R_{anion} (*D*). Vertical dotted lines indicate changes of extracellular conditions. The horizontal dashed line (*B*) serves as a reference for pH 7.2.

at 488 and 458 nm when NO_3^- was added to, or washed out from, the extracellular medium; meanwhile, Cl^- addition had less pronounced effects (*SI Appendix*, Fig. S5). Ratiometric images for R_{pH} and R_{anion} were established from the fluorescence intensity images (Fig. 2 *A* and *C*). The ratiometric maps for R_{pH} and R_{anion} were then used to compute the mean pH_{cyt} (Fig. 2*B*) and the mean R_{anion} in the presence of extracellular NO_3^- and Cl^- for each cell (Fig. 2*D*). The results show that, differently from our observations with NO_3^-, R_{anion} does not change significantly upon addition of Cl^-, suggesting that $[Cl^-]_{cyt}$ was below the range of sensitivity of ClopHensor. In addition, the comparison of pH_{cyt} and R_{anion} changes in the presence of extracellular NO_3^- during the experiment suggests a link between NO_3^- transport and pH modification (Fig. 2 *B* and *D*). Initially (step 1), in the NO_3^--free medium, the pH_{cyt} was 7.01 ± 0.19. Within 35 min, it increased and stabilized to 7.17 ± 0.18, while R_{anion} was constant (Fig. 2*D*). Upon addition of 30 mM extracellular KNO_3 (step 2), the R_{anion} decreased from a mean value in 0 mM NO_3^- of 0.49 ± 0.08 to a value of 0.25 ± 0.03. The calculation of the $[NO_3^-]_{cyt}$ shows that it increased from an initial value of 0.74 ± 0.25 to 4.91 ± 0.40 mM. In parallel, the pH_{cyt} decreased to 6.78 ± 0.04. Both pH_{cyt} and R_{anion} reached a plateau within 20 to 30 min, suggesting a coordination between the two parameters. At step 3, unexpectedly both pH_{cyt} and R_{anion} dropped back to their initial values in less than 4 min after removal of KNO_3. Finally (step 4), when the stomata were exposed to 30 mM KCl, a modest and not significant ($P = 0.17$, $n = 6$) decrease from $pH_{cyt} = 7.17 \pm 0.20$ to $pH_{cyt} = 7.05 \pm 0.40$ was observed, with a rate of pH decrease lower than with 30 mM KNO_3 (Fig. 2*B*). Similar results were obtained when stomata were exposed to KCl only (*SI Appendix*, Fig. S7).

As a whole, these data demonstrate that ClopHensor enables us to simultaneously monitor in vivo the variations in $[Cl^-]_{cyt}$ or $[NO_3^-]_{cyt}$ and pH_{cyt} at a cellular resolution. In the conditions tested, $[Cl^-]_{cyt}$ was below the limit of detection of ClopHensor for Cl^- (i.e., 2 mM) (Fig. 2*D*). This suggests that in our experimental setting, ClopHensor was measuring essentially cytosolic NO_3^- variations. Notably, cytosolic NO_3^- and pH changes appear to be concerted, suggesting that they are governed by a common mechanism.

AtCLCa Accounts for Cytosolic Acidification in Response to NO_3^-. The finding that ClopHensor can measure the dynamic changes of $[NO_3^-]_{cyt}$ and pH_{cyt} in GCs opens the possibility to visualize the activity of intracellular ion transport systems in living cells. We therefore used this sensor to address the role of the vacuolar $2NO_3^-/1H^+$ exchanger AtCLCa in cytosolic NO_3^- and pH homeostasis. AtCLCa is known to mediate the uptake of NO_3^- into the vacuole driven by H^+ extrusion into the cytosol (6, 40). Therefore, based on its biophysical properties, AtCLCa may be involved in the $[NO_3^-]_{cyt}$ and pH_{cyt} responses measured in Fig. 2. To assess this possibility, we generated *clca-3* knockout mutant plants expressing ClopHensor by crossing *clca-3* with a wild-type *pUBI10:ClopHensor* line. Patch-clamp experiments performed on vacuoles isolated from the wild type and *clca-3 pUBI10::ClopHensor* confirmed that *clca-3* plants expressing *pUBI10:ClopHensor* were defective in vacuolar NO_3^- transport activity (*SI Appendix*, Fig. S8). We then compared the dynamic changes of $[NO_3^-]_{cyt}$ and pH_{cyt} in stomata of 14-d-old nitrate-starved seedlings from wild-type and *clca-3 pUBI10:ClopHensor* plants (Figs. 3 and 4). Since AtCLCa is highly selective for NO_3^- over Cl^-, we performed experiments applying extracellular KNO_3 only.

Again, we designed experiments divided in five steps. GCs from the wild type and *clca-3* were 1) perfused with NO_3^--free medium to establish the ratio R^0 of each stomata; 2) perfused with 10 mM KNO_3; 3) washed out with NO_3^--free medium; 4) perfused with 30 mM KNO_3; and 5) washed out with NO_3^--free medium.

Application of this five-step protocol to wild-type *pUBI10:-ClopHensor* GCs showed that $[NO_3^-]_{cyt}$ varies according to the applied extracellular KNO_3 concentration. We calculated the $[NO_3^-]_{cyt}$ to be 1.64 ± 0.32 and 4.74 ± 1.52 mM in 10 and 30 mM KNO_3, respectively ($n = 8$) (Fig. 3 *A*, *B*, and *E*). In the presence of 10 mM KNO_3, the $[NO_3^-]_{cyt}$ reached a plateau in less than 4 min (Fig. 3*B*). However, in the presence of 30 mM KNO_3 in the extracellular medium, the $[NO_3^-]_{cyt}$ rose progressively with a time constant of $\tau = 15 \pm 3$ min (Fig. 3*B*). Interestingly, GCs maintained an $[NO_3^-]$ gradient between the apoplast and the cytosol of about sixfold when either 10 or 30 mM KNO_3 was applied. In all cases, upon washout with NO_3^--free medium, the $[NO_3^-]_{cyt}$ dropped back to concentrations close to the limit of detection within 4 min. In *clca-3 pUBI10:ClopHensor* GCs, the $[NO_3^-]_{cyt}$ behaved similarly to wild-type plants upon exposure to 10 mM KNO_3, reaching 2.24 ± 1.47 mM ($n = 15$) (Fig. 3 *C*–*E*). Further, similarly to the wild type, upon application of 30 mM KNO_3, *clca-3 pUBI10:ClopHensor* GCs $[NO_3^-]_{cyt}$ increased to 6.34 ± 2.91 mM ($n = 15$) (Fig. 3*D*). However, in contrast with the wild type, $[NO_3^-]_{cyt}$ increased faster, reaching a plateau in less than 4 min in *clca-3* ($\tau < 3$ min) compared with about 30 min in wild-type *pUBI10:ClopHensor* GCs (Fig. 3*D*). These data are in agreement with the involvement of the AtCLCa exchanger in buffering cytosolic NO_3^-. Furthermore, we found that the pH_{cyt}

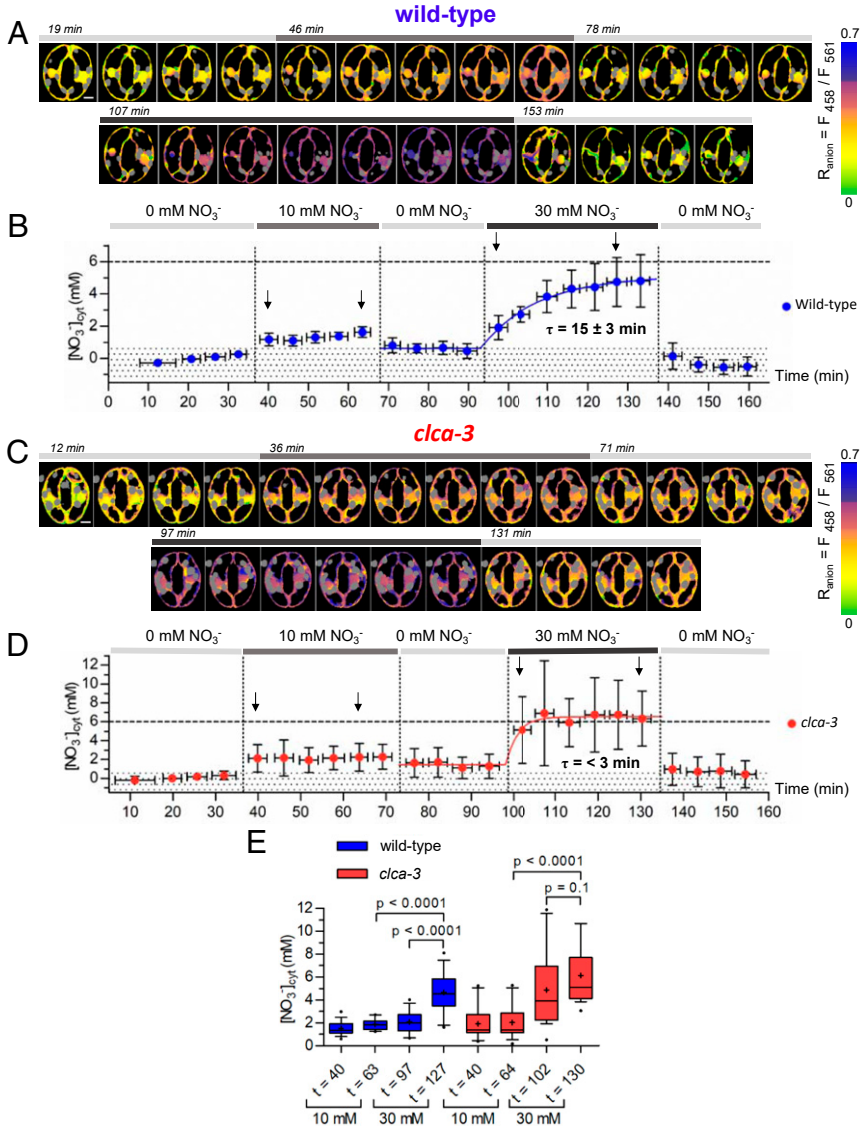

Fig. 3. The vacuolar NO_3^-/H^+ exchanger AtCLCa controls $[NO_3^-]_{cyt}$ in *Arabidopsis* stomata. Epidermal peels from plants grown in vitro for 14 d in NO_3^--free media were imaged (*SI Appendix*). (*A* and *C*) Representative false color ratio images of R_{anion} from wild-type (*A*) and *clca-3* (*C*) stomata at different time points. Stomata were sequentially exposed to 0, 10, and 30 mM KNO_3 (horizontal bar in *Upper*). Gray areas, localization of chloroplasts subtracted during the analysis. (Scale bars: 5 μm.) (*B* and *D*) $[NO_3^-]_{cyt}$ (mean ± SD) at each time point in wild-type (*B*; $n = 8$) and *clca-3* stomata (*D*; $n = 15$). Horizontal error bars represent the time interval of 4 min for the sequential imaging of stomata. Dotted areas, ClopHensor sensitivity threshold for NO_3^-. Vertical dotted lines indicate changes of extracellular conditions. Horizontal dashed lines indicate $[NO_3^-]_{cyt} = 6$ mM. Black arrows, time points used for the box plot analysis in *E*. (*E*) Box plots of the $[NO_3^-]_{cyt}$ at different time points (black arrows in *B* and *D*). Brackets indicate statistically significant differences. Blue boxes, the wild type ($n = 17$); red boxes, *clca-3* ($n = 15$) stomata. Whiskers show the 10 to 90% percentiles. Crosses indicate the means.

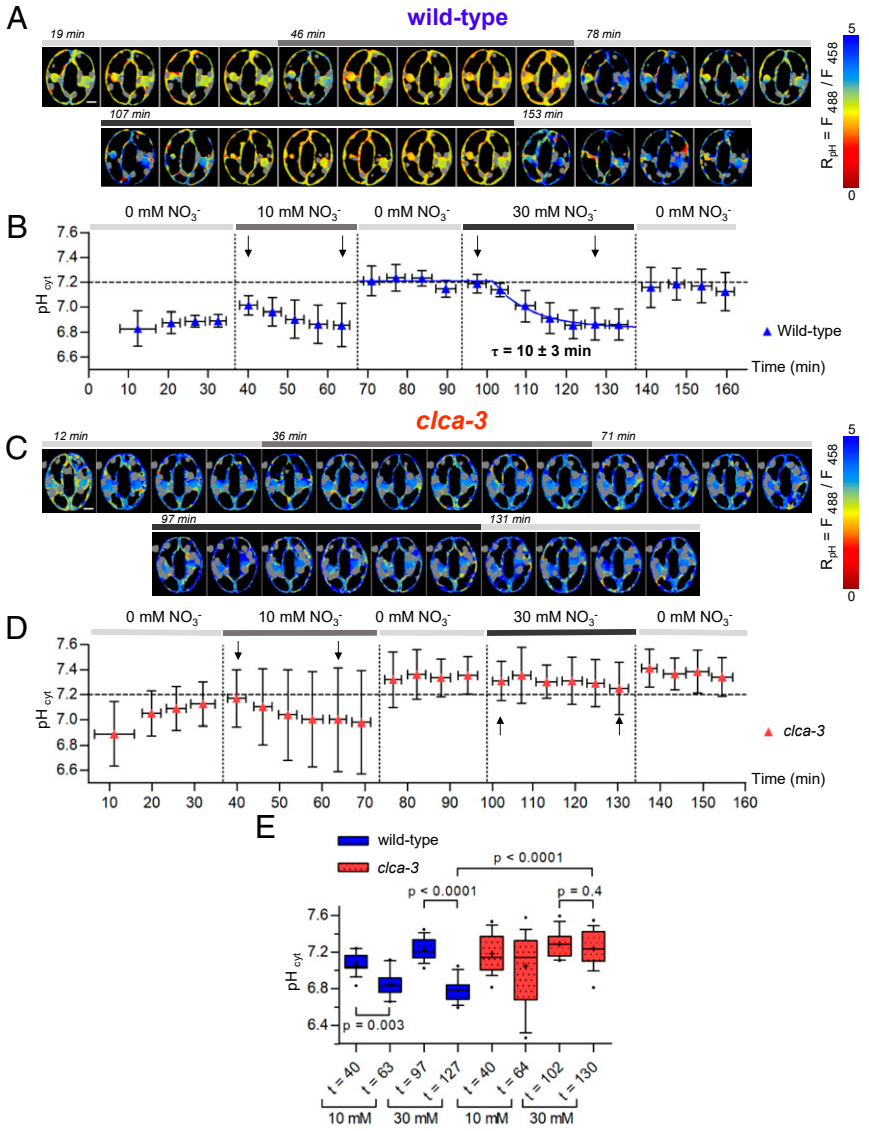

Fig. 4. The vacuolar NO_3^-/H^+ exchanger AtCLCa regulates pH_{cyt} in *Arabidopsis* stomata. Epidermal peels from plants grown in vitro for 14 d in NO_3^--free media were imaged (*SI Appendix*). (*A* and *C*) Representative false color ratio images of R_{pH} from wild-type (*A*) and *clca-3* (*C*) stomata at different time points. Stomata were sequentially exposed to 0, 10, and 30 mM KNO_3 (horizontal bar in *Upper*). Gray areas, localization of chloroplasts subtracted during the analysis. (Scale bars: 5 μm.) (*B* and *D*) pH_{cyt} (mean ± SD) at each time point in wild-type (*B*; $n = 8$) and *clca-3* stomata (*D*; $n = 15$). Horizontal error bars represent the time interval of 4 min for the sequential imaging of stomata. Vertical dotted lines, changes of extracellular conditions. Horizontal dashed lines indicate pH 7.2. Black arrows, time points used for the box plot analysis in *E*. (*E*) Box plots of the pH_{cyt} at different time points (black arrows in *B* and *D*). Brackets indicate statistically significant differences. Blue boxes, the wild type ($n = 17$); red boxes, *clca-3* ($n = 15$). Whiskers show the 10 to 90% percentiles. Crosses indicate the means.

dynamics in the wild type and *clca-3* were markedly different when extracellular KNO_3 was applied (Fig. 4 *A–D*). In wild-type GCs, the pH_{cyt} stabilized at 6.89 ± 0.05 ($n = 8$) at the beginning of the experiments. Then, exposure to 10 mM KNO_3 induced an initial slight pH_{cyt} increase followed by a progressive and modest acidification of the cytosol. Washing out with NO_3^--free medium provoked a fast increase of the pH_{cyt} to 7.21 ± 0.12 ($n = 8$). Then, upon perfusion with 30 mM KNO_3, a progressive and marked acidification to pH 6.87 ± 0.13 ($n = 8$) with a time constant of $\tau = 10 \pm 3$ min was observed. Finally, after washing out in NO_3^--free medium, an alkalinization to 7.16 ± 0.16 ($n = 8$) was observed within 4 min. In *clca-3 pUBI10:ClopHensor* GCs, a modest pH_{cyt} acidification was observed upon exposure to 10 mM KNO_3, as in the wild type. However, this pH_{cyt} decrease was not statistically significant in *clca-3* plants (Fig. 4*E*). Remarkably, the perfusion of 30 mM KNO_3, which induced a marked acidification in wild-type GCs, did not induce any decrease of pH_{cyt} in *clca-3* GCs: pH_{cyt} remained stable at pH ~ 7.3 ($n = 15$) (Fig. 4 *B* and *D*). To exclude an effect of the sequence of KNO_3 application, we inverted step 2 and step 4 in the perfusion protocol and obtained the same results (*SI Appendix*, Fig. S9). These findings show that the presence of the $2NO_3^-/1H^+$ exchanger AtCLCa in the VM is associated with the pH_{cyt} modification detected in wild-type GCs upon perfusion with 30 mM KNO_3, suggesting a role of AtCLCa in the regulation of pH_{cyt}.

We tested whether the application of KNO_3 has an effect on stomata aperture at a whole-leaf level and performed leaf gas exchange measurements on detached leaves (*SI Appendix*, Fig. S10) (41, 42). In these experiments, we applied KNO_3 at the leaf petiole, and we detected an increase of stomata conductance that was similar in the wild type and *clca-3* (*SI Appendix*, Fig. S10 and Table S4). The similar behavior of the wild type and *clca-3* when

KNO_3 is applied converges with the finding that at a cellular level AtCLCa does not determine the steady-state $[NO_3^-]_{cyt}$ (Figs. 3 and 5). The subsequent application of 50 μM ABA on detached leaves induced a similar decrease of the stomata conductance in both the wild type and *clca-3* (*SI Appendix*, Fig. S10 and Table S4). These results with detached leaf gas exchange measurements do not correlate with the observations made on stomata from isolated epidermis from *clca* knockout (7). Such discrepancy between experimental methods and conditions has been reported as well for several well-known knockout mutants involved in ABA signaling and stomata regulation such as, for example, *slac1*, *abi1*, and *abi2* (41).

AtCLCa Is Involved in pH Homeostasis upon Treatment of GCs with Fusicoccin. The results obtained upon treatment with extracellular KNO_3 indicated that AtCLCa may be an important player in pH_{cyt} homeostasis (Figs. 3 and 4). To test whether AtCLCa influences pH_{cyt} regulation independently of the addition of its anion substrates, NO_3^- and Cl^-, we investigated its role in response to the fungal toxin fusicoccin, which triggers stomata opening through a robust activation of the PM H^+ pump (43, 44). In these experiments, we used stomata from plants grown in soil, and since we could not control the initial cellular $[NO_3^-]$ and $[Cl^-]$, we quantified the changes in pH_{cyt} and $[NO_3^-]_{cyt}$ in GCs as $\Delta R_{pH}/R_{pH,i}$ and $\Delta R_{anion}/R_{anion,i}$ (Fig. 5 and *SI Appendix*). Positive values of $\Delta R_{pH}/R_{pH,i}$ and $\Delta R_{anion}/R_{anion,i}$ denote cytosolic alkalinization and increase in $[NO_3^-]_{cyt}$, respectively. To correlate the changes in pH_{cyt} or $[NO_3^-]_{cyt}$ with the opening of stomata, we started the experiments with closed stomata at the end of the dark period (Fig. 5). Thus, epidermal peels from the wild type and *clca-3* were prepared 1 h before the onset of light. After incubation under the microscope for 20 min in a buffer containing 10 mM KNO_3 at pH 5.7, 10 μM fusicoccin was applied for total time of 130 min. Stomata were imaged every 4 min, and we measured pore aperture, R_{pH}, and R_{anion} in each stomata (Fig. 5). Fusicoccin induced a significantly lower opening in *clca-3* (1.8 μm ± 0.1 at 152 min, $n = 15$) compared with wild-type (2.6 μm ± 0.2 at 152 min, $n = 14$) stomata (Fig. 5 *A* and *B*), in agreement with previous results showing that light-induced stomata opening is reduced in *clca* knockout mutants (7). In wild-type stomata, fusicoccin induced a rapid increase of pH_{cyt} leading to a $\Delta R_{pH}/R_{pH,i} = 0.12 \pm 0.02$ as early as 4 min after treatment ($n = 14$) (Fig. 5*C*). Then, pH_{cyt} slowly recovered to almost reach its initial value after 120 min ($\Delta R_{pH}/R_{pH,i} = 0.03 \pm 0.02$, $n = 15$) (Fig. 5*C*). Notably, wild-type stomata not treated with fusicoccin did not open and did not exhibit a significant increase of the

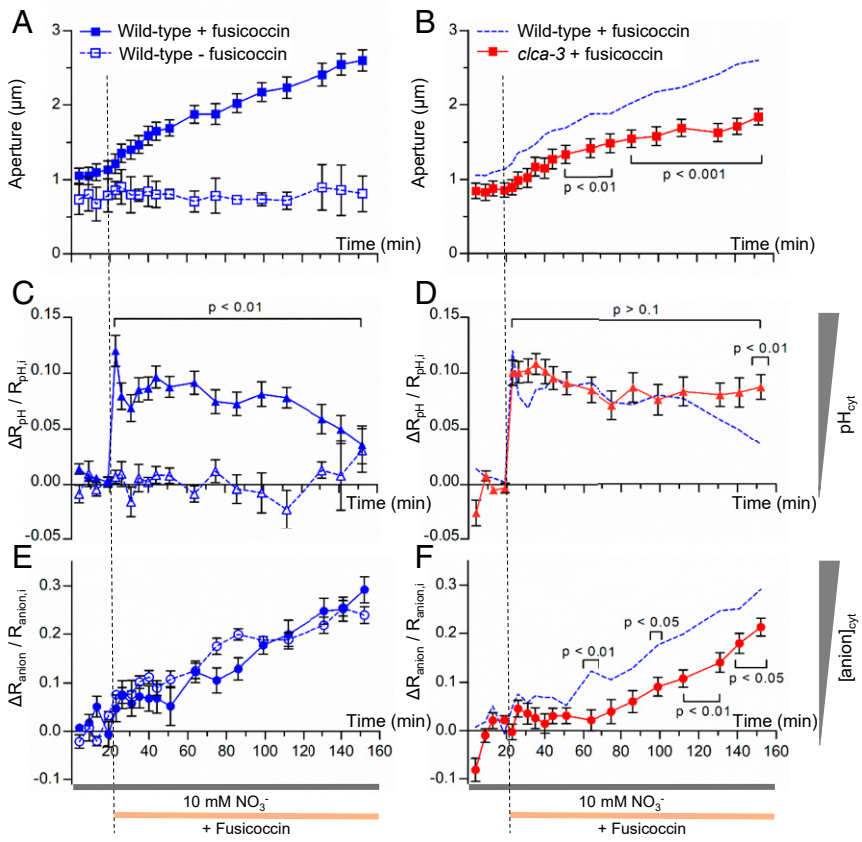

Fig. 5. Fusicoccin-induced pH_{cyt} and $[anion]_{cyt}$ dynamics during stomata opening. (*A* and *B*) Fusicoccin-induced stomata opening from wild-type (*A*) and *clca-3* (*B*) plants expressing ClopHensor. Stomata from epidermal peels were prepared 1 h before light onset and equilibrated for 20 min in the presence of 10 mM KNO_3 before exposure to 10 μM fusicoccin (vertical dotted line) for 120 min or without fusicoccin (dashed lines in *A*, *C*, and *E*). In *clca-3*, fusicoccin induced a significantly lower stomata opening compared with the wild type (dashed lines in *B*, *D*, and *F*; 50 to 80 min $P < 0.01$, 80 to 12 min $P < 0.001$). The stomata in *A* and *B* were imaged to monitor the changes of pH_{cyt} (*C* and *D*) and $[anion]_{cyt}$ (*E* and *F*) during fusicoccin-induced stomata opening. (*C* and *D*) Time-resolved $\Delta R_{pH}/R_{pH,i}$ in wild-type (*C*) and *clca-3* (*D*) stomata. In wild-type (*C*) and *clca-3* (*D*) stomata, the $\Delta R_{pH}/R_{pH,i}$ increased, indicating higher pH_{cyt}. Within 120 min, the $\Delta R_{pH}/R_{pH,i}$ significantly decreased (*C*; $P < 0.01$) in the wild type (*D*) but not in *clca-3* (*D*; $P = 0.45$). (*E* and *F*) Time-resolved $\Delta R_{anion}/R_{anion,i}$ in the wild type (*E*) and *clca-3* (*F*) during fusicoccin-induced stomata opening. In both the wild type + fusicoccin and − fusicoccin, $\Delta R_{anion}/R_{anion,i}$ increased over time, indicating an increase in $[NO_3^-]_{cyt}$. (*F*) In *clca-3*, $\Delta R_{anion}/R_{anion,i}$ increased significantly less than in the wild type (dashed line; $P = 0.02$ after 120 min). In all panels, $n = 14$ for the wild type with fusicoccin, $n = 15$ for *clca-3*, and $n = 5$ for the wild type without fusicoccin. Data are shown as mean ± SEM. Brackets indicate statistically significant differences.

$\Delta R_{pH}/R_{pH,i}$ (n = 5) (Fig. 5*C*). In *clca-3* stomata, fusicoccin induced a rapid increase of pH_{cyt} with a $\Delta R_{pH}/R_{pH,i} = 0.10 \pm 0.01$ after 4 min (n = 14) (Fig. 5*D*) as in the wild type. However, in contrast with the wild type, pH_{cyt} did not recover its initial value in *clca-3* stomata, even after 120 min ($\Delta R_{pH}/R_{pH,i} = 0.09 \pm 0.01$, n = 15) (Fig. 5*D*). The rapid increase in pH_{cyt} observed after fusicoccin treatment (Fig. 5 *C* and *D*) is likely due to the activation of the PM H^+ pumps that are extruding H^+ in the apoplast (43, 44). In *clca-3*, the absence of an NO_3^-/H^+ antiporter pumping H^+ from the vacuole into the cytosol accounts for the defect in pH_{cyt} recovery after fusicoccin-induced alkalinization (6). This result shows that the transport activity of AtCLCa in the VM contributes to the recovery after the cytosolic pH increase induced by fusicoccin. Interestingly, the quantification of $\Delta R_{anion}/R_{anion,i}$ in the wild type

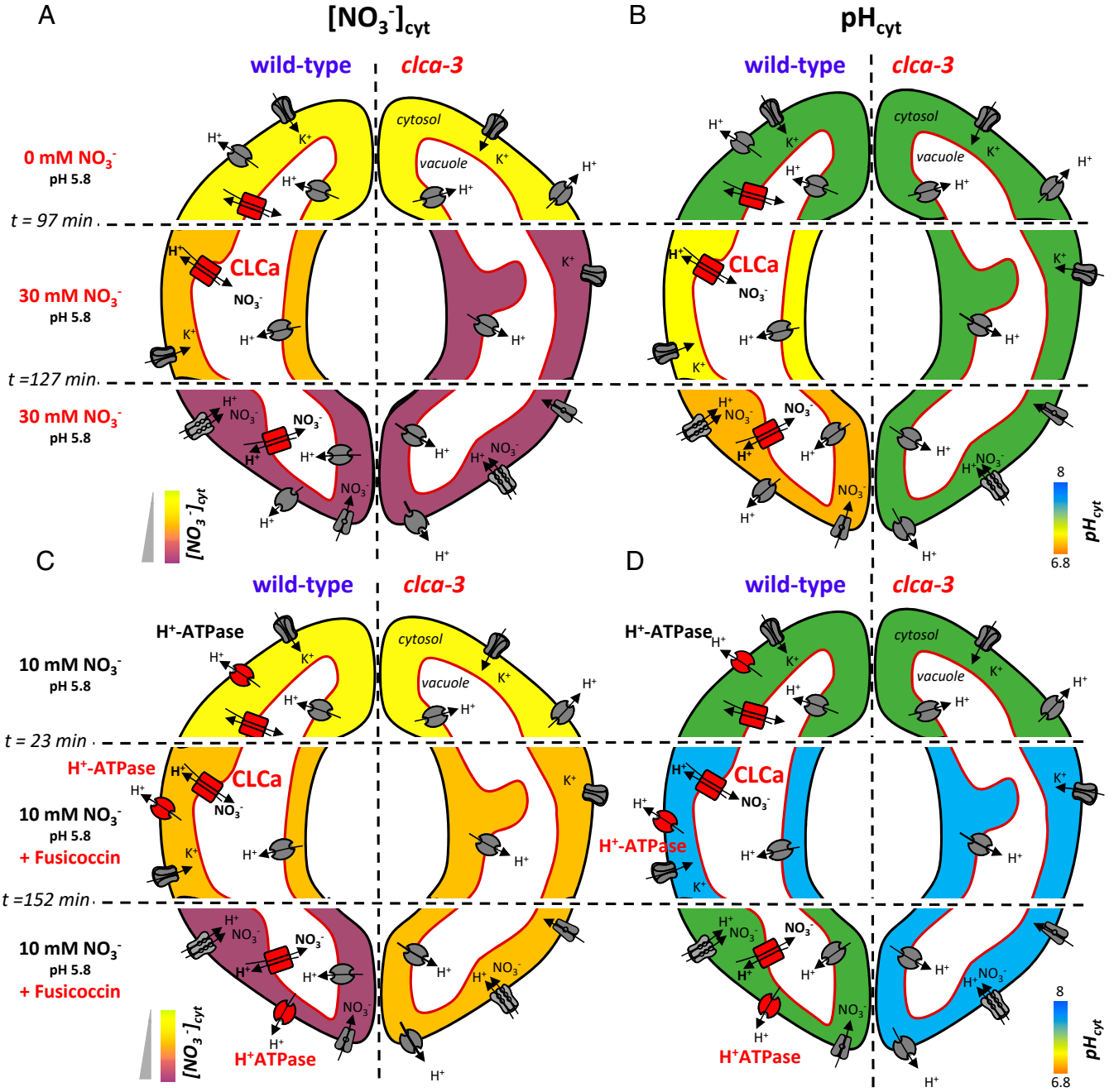

Fig. 6. A vacuolar exchanger modifies cytosolic homeostasis in *Arabidopsis* stomata. Illustration recapitulating the impact of the activity of AtCLCa on $[NO_3^-]_{cyt}$ and pH_{cyt} homeostasis in GCs. (*A*) In the presence of 30 mM KNO_3, NO_3^- enters the cell via NO_3^- transporters and channels residing in the PM. In the wild type (*Left*), the vacuolar AtCLCa exchanger (shown in red) pumps NO_3^- into the vacuole, slowing down $[NO_3^-]_{cyt}$ increase. In the absence of AtCLCa (*Right*), $[NO_3^-]_{cyt}$ stabilizes in less than 4 min. (*B*) In the presence of 30 mM KNO_3, the transport activity of AtCLCa releases H^+ in the cytosol, inducing an acidification in wild-type GCs (*Left*). In the absence of AtCLCa, the cytosolic acidification does not occur (*Right*). (*C* and *D*) Fusicoccin triggers stomata opening, activating the PM H^+-ATPase (shown in red). (*C*) During opening, a progressive increase of $[NO_3^-]_{cyt}$ reaches higher levels in the wild type (*Left*) than in *clca-3* (*Right*). (*D*) Fusicoccin induces an increase of pH_{cyt} in both the wild type (*Left*) and *clca-3* mutant (*Right*). Notably, in the wild type, within 130 min the pH_{cyt} recovers to the initial value (*Left*). Differently, in *clca-3*, the pH_{cyt} did not recover its initial value (*Right*).

showed an increase in $[NO_3^-]_{cyt}$ over the time of the experiment independently of fusicoccin application (Fig. 5*E*). Therefore, increased $[NO_3^-]_{cyt}$ does not seem to determine stomata opening. Intriguingly, the rate of $[NO_3^-]_{cyt}$ increase was significantly lower in *clca-3* than in the wild type (Fig. 5*F*). This is opposite to what one would expect, as AtCLCa removes NO_3^- from the cytosol to store it in the vacuole. This surprising result suggests that a more complex regulation is involved, such as a feedback of the NO_3^- transport capacity of the VM on PM NO_3^- uptake, as previously observed at the whole-plant level (45).

Together, our results strengthen the hypothesis of the role of AtCLCa activity in regulating pH_{cyt} in response not only to fluctuations of extracellular $[NO_3^-]$ but also, to other stimuli such as stomata opening induced by the fungal toxin fusicoccin (Fig. 6). Indeed, in wild-type plants exposed to high $[NO_3^-]$, the dynamics of $[NO_3^-]_{cyt}$ and pH_{cyt} were obviously correlated (compare Fig. 3 *A* and *B* with Fig. 4 *A* and *B*). In contrast, in *clca-3 pUBI10:ClopHensor* GCs, $[NO_3^-]_{cyt}$ changes were not mirrored by pH_{cyt} changes, showing that in *clca-3* the two processes were uncoupled (compare Fig. 3 *C* and *D* with Fig. 4 *C* and *D*). In the case of fusicoccin treatment (Fig. 5), the H^+ import to the cytosol from the vacuole mediated by AtCLCa likely compensates for the increased H^+ extrusion by the PM H^+ pumps. However, the variations of pH_{cyt} and of $[NO_3^-]_{cyt}$ did not display the same kinetics. In contrast, pH_{cyt} recovery seems important for sustained stomata opening. The opening rate was not significantly different between the wild type and *clca-3* during the initial pH increase triggered by fusicoccin, but opening slowed down in *clca-3* compared with the wild type during the pH recovery phase.

Discussion

The involvement of CLCs in severe genetic diseases in humans and their major physiological functions in plants have attracted considerable attention to these anion transport systems. Interestingly, the CLC family presents a dichotomy: the CLCs localized in the PM are anion channels; those localized in intracellular membranes are anion/H^+ exchangers (2). A combination of electrophysiological, structural, and biochemical data provided a detailed understanding of the mechanisms allowing the anion/H^+ exchange or the anion channel behavior at a submolecular level in CLCs (2). However and despite intense research, the cellular function of intracellular CLCs has remained elusive (2). So far, the role of intracellular CLCs was exclusively considered from the point of view of the organelle lumen, while the impact on the *cyt* has been overlooked. Nevertheless, when a CLC exchanger pumps anions into an organelle, it simultaneously releases a stoichiometric amount of H^+ in the cytosol. Therefore, intracellular CLCs have the capacity to influence pH_{cyt} and regulate anionic homeostasis. To test this hypothesis in vivo, we used *Arabidopsis* GCs expressing the dual anion and pH biosensor ClopHensor to unravel the impact of a vacuolar CLC on the cytosol.

ClopHensor Is Able to Sense pH and NO_3^- in Plant Cells. ClopHensor is a genetically encoded biosensor originally developed in mammalian cells. Its photophysical characteristics have been analyzed in depth (34, 46, 47). The advantageous properties of ClopHensor allow us to measure, simultaneously and in the same cell, two important intracellular parameters, pH and the concentration of anions such as Cl^-. Notably, changes in pH and $[Cl^-]$ can report the activity of different types of ion transporters in the VM and PM of plant cells. Before using ClopHensor in plant cells, we first checked its sensitivity toward other anions that, differently from animal cells, are present in the millimolar range in the cytosol (5) (Fig. 1). In vitro analysis demonstrated that ClopHensor is sensitive not only to Cl^- but also, to NO_3^-, while it is insensitive to PO_3^-, malate^{2-}, and citrate^{3-} at the tested concentrations. Furthermore, ClopHensor sensitivity to NO_3^- is even higher than that to Cl^- (Fig. 1). The analysis of the $[NO_3^-]_{cyt}$, $[Cl^-]_{cyt}$, and pH_{cyt} in living GCs demonstrated that ClopHensor is able to report dynamic changes of these parameters (Figs. 3–5). Interestingly, the cytosolic $[NO_3^-]_{cyt}$ we estimated is in the same range as those previously reported in other cell types with selective microelectrodes (35, 48, 49). The agreement between our data and previous reports demonstrates the robustness of ClopHensor to measure $[NO_3^-]_{cyt}$ in *Arabidopsis* GCs. Concerning pH, ClopHensor displays a steep dynamic range fitting cytosolic conditions (Figs. 1, 2, and 4). The steepness of the pH sensitivity is particularly valuable to resolve subtle pH changes. The properties of ClopHensor for pH measurements match those of other pHluorin-derived pH sensors used previously to measure pH_{cyt} in plant cells (50, 51). Overall, our results demonstrate that ClopHensor can be used to measure $[NO_3^-]$ and pH in GCs. Other NO_3^- biosensors have been developed, such as NiTrak, which allows monitoring the activity of the nitrate transporter NRT1.1/NFP5.6 (52), and sNOOOpy, a nitrate/nitrite biosensor that has not been tested in plants yet (53). However, ClopHensor is the first biosensor able to report $[NO_3^-]$ in the cytosol of plants in parallel with pH. Given the link between anion and H^+ transport in plant cells, this dual capacity of ClopHensor is particularly relevant.

A Vacuolar CLC Is Involved in Cytosolic Ion Homeostasis. To reveal the impact of the activity of the vacuolar transporter AtCLCa, we challenged stomata of 14-d-old nitrate-starved seedlings with different extracellular media applied in a defined sequence (Figs. 2–4). Starting from an initial condition with no NO_3^- or Cl^- in the extracellular medium and within the GCs, we applied different KNO_3- and KCl-based media. In our conditions, $[Cl^-]_{cyt}$ was below the sensitivity range of ClopHensor. However, we obtained a remarkable result: $[NO_3^-]_{cyt}$ in GCs can undergo rapid variations (Figs. 2 and 3). To our knowledge, such variations of $[NO_3^-]_{cyt}$ have not been described so far. Former reports available from root epidermal cells or mesophyll protoplasts suggested that $[NO_3^-]_{cyt}$ was stable, at least in the short term (35, 49). These studies were using invasive approaches without challenging cells with modification of the extracellular ion concentrations, possibly explaining why $[NO_3^-]_{cyt}$ changes were not observed. Interestingly, our findings show that $[NO_3^-]_{cyt}$ can change rapidly, within minutes (Figs. 2 and 3). This supports the hypothesis that $[NO_3^-]_{cyt}$ variations may act as an intracellular signal. A role of $[NO_3^-]_{cyt}$ to adjust cell responses to external nitrogen supply has been previously proposed (48, 54). A second remarkable observation we made is a progressive acidification of the cytosol in parallel with the $[NO_3^-]_{cyt}$ increase. Conversely, $[NO_3^-]_{cyt}$ decrease is paralleled by a rapid pH_{cyt} increase (Figs. 2–4 and 6). These findings clearly show a link between $[NO_3^-]_{cyt}$ and pH_{cyt} changes and suggest a common molecular mechanism underlying NO_3^- and pH variations.

The detected changes in pH_{cyt} and $[NO_3^-]_{cyt}$ integrate the transport reactions occurring at the PM and the VM, as well as metabolic reactions and cytosolic buffer capacity. Our data suggest that the observed changes may be due to H^+-coupled transport reactions. In *Arabidopsis* cells, AtCLCa is the major H^+-coupled NO_3^- transporter in the VM (6, 31). Therefore, to test whether AtCLCa is responsible for the variations detected in the cytosol, we conducted comparative experiments between GCs from the wild type and from *clca-3* knockout plants expressing ClopHensor (Figs. 3 and 4). We found that $[NO_3^-]_{cyt}$ reaches a steady-state value faster in *clca-3* GCs than in the wild type when exposed to extracellular KNO_3 (Fig. 3). This proves that in vivo the vacuolar transporter AtCLCa buffers the $[NO_3^-]_{cyt}$, as expected from its function in accumulating NO_3^- into the vacuole (6, 31). This finding may explain the defect of stomata opening reported earlier on isolated epidermis and dehydration test on whole rosettes (7). Gas exchange measurements showed that, on detached leaves, the application of

KNO_3 induces an increase of the stomata conductance with a similar trend in both the wild type and *clca-3* (*SI Appendix*, Fig. S10). Further, in the same experiments both genotypes reacted similarly to the application of ABA. These results seem to be in contrast with the observations made at the level of stomata in isolated epidermis from *clca* knockout (7) (Fig. 5). Such discrepancy is not unique to *clca* mutants as it was reported for other well-known knockout mutants involved in stomata ABA signaling such as, for example, *slac1*, *abi1*, and *abi2* (41). Nevertheless, all these mutants as *clca* display strong defects in tolerance to drought stress at the whole-rosette or whole-plant level. Notably, high concentrations (i.e., 50 μM) of ABA applied at the petiole of detached leaves are required to induce stomata closure in *slac1* and *abi* mutants (41). In such conditions, other anion channels, like ALMT12/QUAC1, may bypass SLAC1 loss of function to allow stomata closure (26).

At the subcellular level, the most impressive consequence of knocking out AtCLCa was on the pH_{cyt} (Fig. 4). Indeed, in sharp contrast with wild-type GCs, no pH acidification could be detected in *clca-3* GCs when $[NO_3^-]_{cyt}$ increased. These unexpected findings reveal that AtCLCa solely accounts for the pH acidification detected in wild-type GCs. Moreover, we found that the absence of AtCLCa also perturbs pH_{cyt} regulation during stomata opening after treatment with fusicoccin (Fig. 5). The role of AtCLCa in the control of pH_{cyt} is therefore not limited to situations involving massive changes of the concentration of its anionic substrate. Together, the results highlight a previously overlooked role of AtCLCa in pH_{cyt} homeostasis. AtCLCa is not the only H^+-coupled transport system operating in the PM and VM of GCs (Fig. 6). However, our results indicate that under the conditions tested, the transport activity of AtCLCa is predominant and high enough to overcome the pH buffering capacity of the cytosol. Therefore, the use of a biosensor like ClopHensor allowed us to detect in vivo the activity of an intracellular transporter, AtCLCa, and its impact of the intracellular ion homeostasis.

The finding that a vacuolar transporter influences pH_{cyt} homeostasis opens a perspective on the cellular functions of intracellular ion transporters. A potential role of H^+-coupled transporters in the regulation of pH_{cyt} was proposed in the '80s (55–57) but was never demonstrated. Instead, the role of intracellular ion transporters is nowadays commonly interpreted from the point of view of the organelle, focusing on how these transporters regulate ion homeostasis in the lumen of the organelles. Our data provide strong experimental evidence supporting the hypothesis that proton-coupled intracellular transporters participate in the regulation of pH_{cyt}. In the plant cell, the VM is commonly considered as a "second layer" with respect to the PM, which is postulated to have a dominant action on intracellular conditions. Our findings show that VM transporters can actively modify the cytosolic conditions rather than "just buffering the cytosol" to maintain homeostatic values. AtCLCa is important in this process, but it might not be the only one (Fig. 6). It will be of interest to understand if and how other transporters like proton pumps or cation/H^+ exchangers (e.g., Na^+/H^+ exchanger [NHX]) as well as ion channels affect cytosolic ion homeostasis.

Cytosolic pH Control, a Framework for CLC Functions. The results presented here relate to a specialized plant cell type, the GCs. The effect of AtCLCa on pH_{cyt} may account for the unexpected defect in stomata closure observed in *clca* knockout plants, while its function in loading anions into the vacuole would rather lead to the prediction that it is solely involved in stomata opening (7). In this context, modification of pH_{cyt} could be an important component of AtCLCa function, as pH_{cyt} is an important parameter in cell signaling (58). The results obtained with fusicoccin argue in favor of this hypothesis. The treatment with fusicoccin was performed on GCs from mature plants, which allowed monitoring changes in stomatal aperture in parallel with pH_{cyt} and $[anion]_{cyt}$ variations. The misregulation of pH_{cyt} in *clca* correlated with the defect in stomata opening. During the initial pH_{cyt} increase that was not affected in *clca*, the rate of stomata opening was similar in the wild type and *clca*. In the following phase, the defect in pH_{cyt} recovery in *clca* mutant paralleled a drop in the rate of stomata opening. Cytosolic pH modifications may modulate ion transport systems and enzymatic reactions to trigger stomata opening or closure. For example, the activity of vacuolar H^+ ATPase (V-ATPase) is modified by changes of the pH_{cyt} (59). Our findings may also be relevant in the broader context of other eukaryotic CLC exchangers. Indeed, the function of intracellular CLCs has been interpreted assuming that their only role was to regulate the lysosomal, endosomal, or vacuolar lumen conditions (2). However, the cellular functions of the lysosomal CLC-7 and endosomal CLC-5 remain unclear in mammal cells. CLC-7 was proposed to acidify the lysosomal lumen, but only modest and controversial effects were detected (14, 16). In the case of CLC-5, endosomes from knockout mice present impaired luminal acidification (33). Nonetheless, the connection between endosomal acidification and the severe defects caused by CLC-5 mutations in Dent's disease is still unclear (2). Indeed, renal failure associated with some mutations in CLC-5 present impaired endocytosis in tubular cells, which is independent of endosomal acidification (33). Intriguingly, pH_{cyt} is known to affect endocytosis (60, 61). The results we report here suggest that in eukaryotic cells, intracellular CLCs are part of the cytosolic pH balance machinery. These findings open a perspective on the function of these exchangers in eukaryotic cells and may provide a framework to understand the pathophysiological disorders caused by mutations in human CLC genes.

Methods

Wild-type *Arabidopsis* plants were Col-0 ecotype. The *clca-3* knockout line corresponds to Gabi Kat GK-624E03-022319. Images were acquired with a Leica SP8 upright CLSM. Image analysis was performed with ImageJ. Detailed description of the methods is available in *SI Appendix*.

Data Availability. All data presented in the paper are described in the text and *SI Appendix*. Biological materials are available from the corresponding author on request.

ACKNOWLEDGMENTS. This work was supported by LabEx Saclay Plant Sciences-SPS (ANR-10-LABX-0040-SPS) and by the ATIP-AVENIR-2018 program. P.C.-F. was supported by a postdoctoral grant from Fundacion Alfonso Martin Escudero. This work has benefited from the facilities and the expertise of Imagerie-Gif microscopy platform, which is supported by France-BioImaging (ANR-INBS-04 "Investments for the future") and by Saclay Plant Science (ANR-11 IDEX-0003-02). We thank M. Dauzat (Laboratoire d'Ecophysiologie des Plantes sous Stress Environnementaux) and N. Sidibé (Institute for Integrative Biology of the Cell) for the help with experiments, Joni Frederick for reading the manuscript, D. Arosio (Consiglio Nazionale delle Ricerche) for providing plasmid with ClopHensor and advice, R. Le Bars (Imagerie-Gif) for the help with microscopy, and M. Bianchi (Institute for Integrative Biology of the Cell) and S. Filleur (Institute for Integrative Biology of the Cell) for discussion.

1. P. B. Persson, A. Bondke Persson, Channels and channelopathies. *Acta Physiol. (Oxf.)* **218**, 149–151 (2016).
2. T. J. Jentsch, M. Pusch, CLC chloride channels and transporters: Structure, function, physiology, and disease. *Physiol. Rev.* **98**, 1493–1590 (2018).
3. E. Park, R. MacKinnon, Structure of the CLC-1 chloride channel from *Homo sapiens*. *eLife* **7**, e36629 (2018).
4. R. Dutzler, E. B. Campbell, M. Cadene, B. T. Chait, R. MacKinnon, X-ray structure of a ClC chloride channel at 3.0 A reveals the molecular basis of anion selectivity. *Nature* **415**, 287–294 (2002).
5. D. Geelen *et al*., Disruption of putative anion channel gene AtCLC-a in *Arabidopsis* suggests a role in the regulation of nitrate content. *Plant J.* **21**, 259–267 (2000).
6. A. De Angeli *et al*., The nitrate/proton antiporter AtCLCa mediates nitrate accumulation in plant vacuoles. *Nature* **442**, 939–942 (2006).
7. S. Wege *et al*., Phosphorylation of the vacuolar anion exchanger AtCLCa is required for the stomatal response to abscisic acid. *Sci. Signal.* **7**, ra65 (2014).
8. M. Jossier *et al*., The *Arabidopsis* vacuolar anion transporter, AtCLCc, is involved in the regulation of stomatal movements and contributes to salt tolerance. *Plant J.* **64**, 563–576 (2010).

9. C. T. Nguyen *et al*., Characterization of the chloride channel-like, AtCLCg, involved in chloride tolerance in *Arabidopsis thaliana*. *Plant Cell Physiol.* **57**, 764–775 (2016).
10. J. Böhm *et al*., Understanding the molecular basis of salt sequestration in epidermal bladder cells of *Chenopodium quinoa*. *Curr. Biol.* **28**, 3075–3085.e7 (2018).
11. A. Herdean *et al*., The *Arabidopsis* thylakoid chloride channel AtCLCe functions in chloride homeostasis and regulation of photosynthetic electron transport. *Front. Plant Sci.* **7**, 115 (2016).
12. A. Accardi, C. Miller, Secondary active transport mediated by a prokaryotic homologue of ClC Cl- channels. *Nature* **427**, 803–807 (2004).
13. A. Picollo, M. Pusch, Chloride/proton antiporter activity of mammalian CLC proteins ClC-4 and ClC-5. *Nature* **436**, 420–423 (2005).
14. A. R. Graves, P. K. Curran, C. L. Smith, J. A. Mindell, The Cl-/H+ antiporter ClC-7 is the primary chloride permeation pathway in lysosomes. *Nature* **453**, 788–792 (2008).
15. A. A. Zdebik *et al*., Determinants of anion-proton coupling in mammalian endosomal CLC proteins. *J. Biol. Chem.* **283**, 4219–4227 (2008).
16. S. Weinert *et al*., Lysosomal pathology and osteopetrosis upon loss of H+-driven lysosomal Cl– accumulation. *Science* **328**, 1401–1403 (2010).
17. M. R. G. Roelfsema, R. Hedrich, In the light of stomatal opening: New insights into "the Watergate.". *New Phytol.* **167**, 665–691 (2005).
18. T.-H. Kim, M. Böhmer, H. Hu, N. Nishimura, J. I. Schroeder, Guard cell signal transduction network: Advances in understanding abscisic acid, CO2, and Ca2+ signaling. *Annu. Rev. Plant Biol.* **61**, 561–591 (2010).
19. E. A. G. MacRobbie, Signal transduction and ion channels in guard cells. *Philos. Trans. R. Soc. Lond. B Biol. Sci.* **353**, 1475–1488 (1998).
20. Z. Andrés *et al*., Control of vacuolar dynamics and regulation of stomatal aperture by tonoplast potassium uptake. *Proc. Natl. Acad. Sci. U.S.A.* **111**, E1806–E1814 (2014).
21. A. De Angeli, J. Zhang, S. Meyer, E. Martinoia, AtALMT9 is a malate-activated vacuolar chloride channel required for stomatal opening in *Arabidopsis*. *Nat. Commun.* **4**, 1804 (2013).
22. T. Vahisalu *et al*., SLAC1 is required for plant guard cell S-type anion channel function in stomatal signalling. *Nature* **452**, 487–491 (2008).
23. J. Negi *et al*., CO2 regulator SLAC1 and its homologues are essential for anion homeostasis in plant cells. *Nature* **452**, 483–486 (2008).
24. H. Zhang *et al*., Two tonoplast MATE proteins function as turgor-regulating chloride channels in *Arabidopsis*. *Proc. Natl. Acad. Sci. U.S.A.* **114**, E2036–E2045 (2017).
25. M. Jezek, M. R. Blatt, The membrane transport system of the guard cell and its integration for stomatal dynamics. *Plant Physiol.* **174**, 487–519 (2017).
26. S. Meyer *et al*., AtALMT12 represents an R-type anion channel required for stomatal movement in *Arabidopsis* guard cells. *Plant J.* **63**, 1054–1062 (2010).
27. C. Eisenach *et al*., ABA-induced stomatal closure involves ALMT4, a phosphorylation-dependent vacuolar anion channel of *Arabidopsis*. *Plant Cell* **29**, 2552–2569 (2017).
28. J. Zhang *et al*., Identification of SLAC1 anion channel residues required for CO_2/bicarbonate sensing and regulation of stomatal movements. *Proc. Natl. Acad. Sci. U.S.A.* **115**, 11129–11137 (2018).
29. D. Geiger *et al*., Stomatal closure by fast abscisic acid signaling is mediated by the guard cell anion channel SLAH3 and the receptor RCAR1. *Sci. Signal.* **4**, ra32 (2011).
30. V. Barragán *et al*., Ion exchangers NHX1 and NHX2 mediate active potassium uptake into vacuoles to regulate cell turgor and stomatal function in *Arabidopsis*. *Plant Cell* **24**, 1127–1142 (2012).
31. S. Wege *et al*., The proline 160 in the selectivity filter of the *Arabidopsis* NO(3)(–)/H(+) exchanger AtCLCa is essential for nitrate accumulation in planta. *Plant J.* **63**, 861–869 (2010).
32. A. Carpaneto, A. Boccaccio, L. Lagostena, E. Di Zanni, J. Scholz-Starke, The signaling lipid phosphatidylinositol-3,5-bisphosphate targets plant CLC-a anion/H^+ exchange activity. *EMBO Rep.* **18**, 1100–1107 (2017).
33. G. Novarino *et al*., Endosomal chloride-proton exchange rather than chloride conductance is crucial for renal endocytosis. *Science* **328**, 1398–1401 (2010).
34. D. Arosio *et al*., Simultaneous intracellular chloride and pH measurements using a GFP-based sensor. *Nat. Methods* **7**, 516–518 (2010).
35. S. J. Cookson, L. E. Williams, A. J. Miller, Light-dark changes in cytosolic nitrate pools depend on nitrate reductase activity in *Arabidopsis* leaf cells. *Plant Physiol.* **138**, 1097–1105 (2005).
36. J. M. Frachisse, S. Thomine, J. Colcombet, J. Guern, H. Barbier-Brygoo, Sulfate is both a substrate and an activator of the voltage-dependent anion channel of *Arabidopsis* hypocotyl cells. *Plant Physiol.* **121**, 253–262 (1999).
37. H. H. Felle, The H+/Cl– symporter in root-hair cells of sinapis alba (An electrophysiological study using ion-selective microelectrodes). *Plant Physiol.* **106**, 1131–1136 (1994).
38. A. J. Miller, X. Fan, M. Orsel, S. J. Smith, D. M. Wells, Nitrate transport and signalling. *J. Exp. Bot.* **58**, 2297–2306 (2007).
39. N. Leonhardt *et al*., Microarray expression analyses of *Arabidopsis* guard cells and isolation of a recessive abscisic acid hypersensitive protein phosphatase 2C mutant. *Plant Cell* **16**, 596–615 (2004).
40. E. Y. Bergsdorf, A. A. Zdebik, T. J. Jentsch, Residues important for nitrate/proton coupling in plant and mammalian CLC transporters. *J. Biol. Chem.* **284**, 11184–11193 (2009).
41. F. Pantin *et al*., The dual effect of abscisic acid on stomata. *New Phytol.* **197**, 65–72 (2013).
42. P. H. O. Ceciliato *et al*., Intact leaf gas exchange provides a robust method for measuring the kinetics of stomatal conductance responses to abscisic acid and other small molecules in *Arabidopsis* and grasses. *Plant Methods* **15**, 38 (2019).
43. M. Marra *et al*., The fungal H(+)-ATPase from *Neurospora crassa* reconstituted with fusicoccin receptors senses fusicoccin signal. *Proc. Natl. Acad. Sci. U.S.A.* **92**, 1599–1603 (1995).
44. F. Johansson, M. Sommarin, C. Larsson, Fusicoccin activates the plasma membrane H+-ATPase by a mechanism involving the C-terminal inhibitory domain. *Plant Cell* **5**, 321–327 (1993).
45. D. Monachello *et al*., Two anion transporters AtClCa and AtClCe fulfil interconnecting but not redundant roles in nitrate assimilation pathways. *New Phytol.* **183**, 88–94 (2009).
46. D. Arosio *et al*., Spectroscopic and structural study of proton and halide ion cooperative binding to GFP. *Biophys. J.* **93**, 232–244 (2007).
47. R. Bizzarri *et al*., Development of a novel GFP-based ratiometric excitation and emission pH indicator for intracellular studies. *Biophys. J.* **90**, 3300–3314 (2006).
48. A. J. Miller, S. J. Smith, Cytosolic nitrate ion homeostasis: Could it have a role in sensing nitrogen status? *Ann. Bot.* **101**, 485–489 (2008).
49. M. Van Der Leij, S. J. Smith, A. J. Miller, Remobilisation of vacuolar stored nitrate in barley root cells. *Planta* **205**, 64–72 (1998).
50. A. Martinière, G. Desbrosses, H. Sentenac, N. Paris, Development and properties of genetically encoded pH sensors in plants. *Front. Plant Sci.* **4**, 523 (2013).
51. A. Martinière *et al*., Uncovering pH at both sides of the root plasma membrane interface using noninvasive imaging. *Proc. Natl. Acad. Sci. U.S.A.* **115**, 6488–6493 (2018).
52. C. H. Ho, W. B. Frommer, Fluorescent sensors for activity and regulation of the nitrate transceptor CHL1/NRT1.1 and oligopeptide transporters. *eLife* **3**, e01917 (2014).
53. M. Hidaka *et al*., Visualization of $NO3^-$/$NO2^-$ dynamics in living cells by fluorescence resonance energy transfer (FRET) imaging employing a rhizobial two-component regulatory system. *J. Biol. Chem.* **291**, 2260–2269 (2016).
54. A. Krapp, Plant nitrogen assimilation and its regulation: A complex puzzle with missing pieces. *Curr. Opin. Plant Biol.* **25**, 115–122 (2015).
55. F. A. Smith, J. A. Raven, Intracellular pH and its regulation. *Annu. Rev. Plant Physiol.* **30**, 289–311 (1979).
56. A. Kurkdjian, J. Guern, Intracellular pH: Measurement and importance in cell activity. *Annu. Rev. Plant Physiol. Plant Mol. Biol.* **40**, 271–303 (1989).
57. H. H. Felle, pH: Signal and messenger in plant cells. *Plant Biol.* **3**, 577–591 (2001).
58. S. Behera *et al*., Cellular Ca2+ signals generate defined pH signatures in plants. *Plant Cell* **30**, 2704–2719 (2018).
59. F. Rienmüller *et al*., Luminal and cytosolic pH feedback on proton pump activity and ATP affinity of V-type ATPase from *Arabidopsis*. *J. Biol. Chem.* **287**, 8986–8993 (2012).
60. K. Sandvig, S. Olsnes, O. W. Petersen, B. van Deurs, Inhibition of endocytosis from coated pits by acidification of the cytosol. *J. Cell. Biochem.* **36**, 73–81 (1988).
61. K. Sandvig, S. Olsnes, O. W. Petersen, B. van Deurs, Acidification of the cytosol inhibits endocytosis from coated pits. *J. Cell Biol.* **105**, 679–689 (1987).